

# Microstructural Analysis of Laser Coated Ceramic Components TiB<sub>2</sub> and TiC on Aluminium Alloy EN AW-6082-T651

Dunja Ravnikar<sup>1</sup> – Primož Mrvar<sup>2</sup> – Jožef Medved<sup>2</sup> – Janez Grum<sup>1,\*</sup>

<sup>1</sup> University of Ljubljana, Faculty of Mechanical Engineering, Slovenia

<sup>2</sup> University of Ljubljana, Faculty of Natural Science in Engineering, Slovenia

*This paper deals with the deposition of ceramic powder coating TiB<sub>2</sub>-TiC mix with aluminium powder on the 6082-T651 aluminium alloy by means of laser coating. The resulting coating was studied by means of a microstructural and microchemical analysis. Microhardness was measured in the coating and in the substrate area under the coating. A thermodynamic analysis of the system showed the potential existence of aluminium carbide Al<sub>4</sub>C<sub>3</sub> in the coating, whereas the EDS analysis indicated a possible occurrence of aluminium oxycarbides in the coating, containing TiB<sub>2</sub>, TiC and Al. An additional thermal analysis explained the existence of two separate exothermic peaks, on the basis of which it could be inferred that the precipitation of phase Mg<sub>2</sub>Si, which is a typical precipitate in aluminium alloy 6082, occurred. Microhardness measurements confirmed the differences in the hardness of the coating, resulting from different energy input during the coating process. Due to the thermal effect of the coating process and the rapid cooling of the coating and the coating-substrate interface, microstructural changes occurred on the substrate surface under the coating. The modified microstructure under the coating resulted in reduced hardness, which could be attributed to the use of the alloys in the precipitation-hardened state. Thermal effects of the coating process and rapid cooling contributed to the occurrence of forced dissolution with reduced microhardness.*

**Keywords:** laser coating, aluminium alloy EN AW 6082-T651, ceramic components TiC-TiB<sub>2</sub>, microstructure, microhardness

## 0 INTRODUCTION

Aluminium alloys used in specific applications have to meet set operating requirements. Therefore, they are frequently heat-treated or hardened through cold deformation in order to obtain the desired surface properties. Surface engineering may be used to improve the required mechanical and chemical properties of different substrate materials. Žagar and Grum [1] report the improved resistance of aluminium alloys 6082-T651 and 2007-T351 to fatigue, resulting from micromechanical hardening of the surface by means of shot peening. The improved mechanical properties and resistance to corrosion of aluminium alloy 6082-T651, obtained through laser shock peening, were observed by Trdan et al. [2] and [3]. Sušnik et al. [4] reported the increased hardness of the surface layer of aluminium alloy AlSi12CuNiMg, achieved via laser surface remelting. Nowadays, surface properties are frequently modified by means of laser coating, while the desired mechanical and chemical properties of the surface are obtained through the application of the coating by remelting the powder components and thin substrate layer. The application of different ceramic components may also increase the wear resistance of the surface of aluminium alloys [5] to [7]. Aluminium alloys coated with ceramic components contribute to the reduced weight of a device or a machine. The laser coating of aluminium alloys by means of metal-matrix composites is becoming ever more appealing for the application in the automotive and chemical

processing industry. Light construction materials with coatings that improve their properties may represent a significant technological advance in the field of surface engineering, as they may be the alternatively used in the design of light engines with improved efficiency [8].

The only issue with products with such coatings is related to the bonding of ceramic components with a high melting point to aluminium, which has a significantly lower melting point. Therefore, the process of preparing the surface and applying the ceramic powder components during the laser heating process is particularly important. What is also important in the application of coatings on aluminium alloys is the composition of ceramic powder components with additives that have to enable good wettability during the remelting of pre-deposited powder on the substrate. Therefore, complementary additives are added to ceramic components in view of the substrate type with the purpose of improving the coating-substrate interface under the resulting ceramic coating and the substrate surface. Katipelli et al. [5] subjected the AlMg1SiCu aluminium alloy to laser coating, whereas the surface was coated with titanium carbide to which 10% of Si was added, improving the wettability and fluidity of the resulting melt, enabling better adhesion of the coating to the substrate, and facilitating the filling of pores in the coating and in the coating-substrate interface that occur during the coating process. Chong et al. [6] coated the same aluminium alloy with a precursor of titanium carbide

\*Corr. Author's Address: University of Ljubljana, Faculty of Mechanical Engineering, Aškerčeva 6, 1000 Ljubljana, Slovenia, janez.grum@fs.uni-lj.si

and molybdenum; different component ratios were used. The results showed an improved wear resistance of the coating, especially with the ratio of 70% of TiC and 30% of Mo. Better adhesion of the coated layer to the substrate can be obtained by adding metal powder particles to ceramic components. These particles must have a lower melting point, such as aluminium or copper [9]. With the transition of a low-energy laser beam across the pre-deposited powder, only the component with the lower melting point is fully melted. Thus, the re-melted metal matrix with a low melting point and the respective precipitates appear in the coating, together with dispersed solid particles. Following the solidification, a metal composite coating with solid refractory particles emerges, providing the desired mechanical and chemical properties [9].

In numerous studies, aluminium alloys were coated with powder precursors of Al-Si [8] and [10] or Al-Ti [11], reinforced with TiC and TiB<sub>2</sub> particles. Dubourg et al. [8] applied different ratios of Al-Si powder and TiC to pure aluminium. It was established that higher contents of Si and TiC increase the hardness of the coated layer. Wear tests revealed a poor wear resistance of sub-eutectic alloys with less than 12 % wt. of Si, with no TiC present. A slight increase of the wear resistance of sub-eutectic alloys was achieved with the addition of TiC. Uenishi and Kobayashi [11] applied powder precursor Al-25% Ti with the addition of TiC, TiB<sub>2</sub> and SiC (the content of up to 40%) to pure aluminium. When TiB<sub>2</sub> was added, it melted, resulting in a homogeneous coating of Al<sub>3</sub>Ti / TiB<sub>2</sub> with finely dispersed ceramic particles. However, the addition of TiC made melting more difficult. The particles were thus dispersed in the Al<sub>3</sub>Ti matrix. The authors concluded that, at the highest available laser power density of 2.5 kW and with the addition of 40% of TiC, the Al<sub>3</sub>Ti / TiC coating with a good interface to the substrate emerges. In contrast, other authors report that the same laser power density and 40% of TiB<sub>2</sub> do not result in good adhesion of the Al<sub>3</sub>Ti / TiB<sub>2</sub> coating to the substrate. Anandkumar et al. [10] coated alloy Al-7 wt.% of Si with powder precursor Al-12 wt.% Si and 40 wt.% of TiB<sub>2</sub>. Increased hardness of the coated layer, i.e. 156 HV<sub>0.1</sub>, and a relatively low specific wear rate of  $2.65 \times 10^{-5}$  mm<sup>3</sup>/Nm was obtained. Their finding was extremely valuable, namely that during the remelting of metal and ceramic components no chemical reactions occurred between the molten aluminium and TiB<sub>2</sub>. That means that no dissolution of TiB<sub>2</sub> took place. Similar experiments were conducted on titanium alloys, where there were also no chemical reactions between the molten titanium and TiB<sub>2</sub> [6]. TiB<sub>2</sub> particles remained unevenly distributed in the

resulting coating, which could be attributed to different powder and alloy densities [6]. The application of precursor of Al-Si and Ni, with the addition of TiC, on the Al-Si aluminium alloy also did not result in any TiC dissolution. Due to considerable differences in the powder and alloy densities, the particles remained unevenly distributed in the resulting coating [6].

## 1 EXPERIMENTAL PROCEDURE

### 1.1 Material Selection

The substrate material chosen for the study was EN AW 6082-T651 aluminium alloy; its chemical composition is given in Table 1, and mechanical properties are presented in Table 2. The first part of the designation, i.e. 6082, indicates that this alloy belongs to the 6000 series alloys, whose main alloying elements are silicon and magnesium. The second part of the designation, i.e. T651, indicates the alloy's temper. The alloy underwent a homogenization annealing at a temperature of  $525 \pm 15$  °C and additional cold deformation after quenching. It was then subjected to artificial ageing at temperatures between 165 and 195 °C for 3 to 12 h [12].

The following powder precursors with aluminium were chosen for the clad material:

- TiB<sub>2</sub> with a purity of 99.5% and average particle size of 45 µm;
- TiC with a purity of 99.5% and average particle size of 2 µm;
- Al with a purity of 99.5% and average particle size of 45 µm.

The powders were obtained from Global Tungsten & Powder Corp.

Two different ratios of powder precursor were chosen:

- 40 wt.% TiB<sub>2</sub> - 40 wt.% TiC - 20 wt.% Al,
- 60 wt.% TiB<sub>2</sub> - 20 wt.% TiC - 20 wt.% Al,

to determine the physical and chemical properties of the coated layer as well as of the coating-substrate interface. Aluminium was added to TiB<sub>2</sub>-TiC ceramic components to improve the adhesion of the ceramic coating to the substrate, following the laser heating and remelting process.

### 1.2 Specimen Preparation

With the use of the water jet process, flat aluminium specimens with dimensions of 25 × 50 × 10 mm were cut from a rolled sheet with a thickness of 10 mm. Prior to powder precursor deposition, the specimen surface was sanded with SiC sandpaper with a grit

Table 1. Chemical composition of EN AW 6082 aluminium alloy [13]

	Si [wt.%]	Mg [wt.%]	Mn [wt.%]	Fe [wt.%]	Cr [wt.%]	Zn [wt.%]	Ti [wt.%]	Cu [wt.%]
ENAW 6082	0.7 to 1.3	0.6 to 1.2	0.4 to 1.0	≤ 0.5	≤ 0.25	≤ 0.2	≤ 0.10	≤ 0.10

Table 2. Mechanical properties of EN AW 6082 aluminium alloy [14]

AA designation	Alloy temper	Rm [MPa]	Rp <sub>0.2</sub> [MPa]	A [%]	HBW
6082	T651	min. 260 to 310	min. 220 to 260	min. 2 to 10	83 to 94

Table 3: Laser coating parameters

Specimen designation	Clad material		Laser traverse speed [mm/s]	Overlapping rate [%]	Laser beam power [W]	Energy density [J/mm <sup>2</sup> ]
	Type	Ratio [wt.%]				
#1	TiB <sub>2</sub> / TiC / Al	40 / 40 / 20	60	50	800	13.33
#2					1000	16.67
#3					1200	20.00
#4					800	13.33
#5					1000	16.67
#6					1200	20.00
#7		60 / 20 / 20	60	50	800	13.33
#8					1000	16.67
#9					1200	20.00
#10					800	13.33
#11					1000	16.67
#12					1200	20.00

of 600 and then subjected to ultrasonic cleaning in methanol. The precursor powders were mixed with a water-based organic binder (LISI W 1583) and reducer (LISI W15833) obtained from the Warren Paint and Color Company. The prepared powder precursor with the binder and reducer was then spray-deposited on a chemically clean surface of the aluminium alloy with an estimated coating thickness of 150±25 µm. The sprayed specimens were then dried for one day at room temperature.

### 1.3 Laser Coating

To provide good chemical bonding between the coated layer and substrate, a sufficient energy input had to be provided to re-melt the pre-deposited powder and partially also the substrate. A 3-kW IPG Photonics continuous wave fibre laser with a wavelength of 1070 nm was employed. The focus of the laser beam to the specimen surface was such as to provide a uniform spot size of 1.0 mm diameter. Regarding the desired temperature and time conditions, three different laser beam power values were chosen: 800, 1000 and 1200 W. The traverse speed of the laser beam was constant, i.e. 60 mm/s, for all laser-re-

melted specimens, enabling sufficient energy input of 13.33, 16.67 and 20.00 J/mm<sup>2</sup> with regard to the spot size and selected laser beam power values. Two different overlapping rates of individual laser tracks on the specimen surface were selected: 30 and 50%. The coating was applied to twelve specimens. The coating parameters are given in Table 3.

## 2 RESULTS AND DISCUSSION

### 2.1 Microstructural Analysis Supported by EDS Analysis

The coated specimens for metallographic analysis were cut on a special-purpose cutting machine and mounted in Polyfast Phenolic hot mountain resin with carbon filter (Struers). Specimens were then gradually sanded with SiC sandpaper with grits from 220 to 800. The sanding and polishing process is rather demanding due to the treated elemental aluminium. Therefore, the controlled sanding conditions were chosen as follows: a set normal force of 180 N, sandpaper with a grit of 220, and a 2 min period of sanding. The period of sanding with sandpapers with grits of 500 and 800 was 1 min for each grit size. The process was followed by a 3 min polishing with a 3.0 µm diamond

paste and a force of 180 N, and a 1 min final polishing with a 1.0  $\mu\text{m}$  paste and a force of 100 N. An aqueous solution of 2 ml HF + 3 ml HCl + 5 ml HNO<sub>3</sub> + 90 ml H<sub>2</sub>O was used as the etchant. Microstructural analysis was conducted on scanning electron microscopes Nova™ NanoSEM 230 and JEOL JSM-6500F, followed by the EDS analysis. The thickness of the coating and its porosity were determined by means of an Orthoplan optical microscope at a magnification of 100 $\times$ .

Fig. 1a shows an image of the cross-section of specimen #1, captured with the electron microscope at a magnification of 150 $\times$ . The specimen was coated with a 40 / 40 / 20 ratio of clad material, an overlapping rate of 50% and an energy density of 13.3 J/mm<sup>2</sup>. The image shows good adhesion of the coating to the substrate with no cracks and low porosity. It is of utmost importance that good adhesion of the coating to the substrate be obtained with all combinations of laser coating parameters. The method of the pre-deposition of the clad material to the substrate surface resulted in the anticipated coating thickness deviations, which,

however, have no significant effect on further results. The average thickness of the coating measured in all the coated specimens amounted to about 130  $\mu\text{m}$ . The lowest average thickness of the coating was measured in specimen #10, amounting to 80.50  $\mu\text{m}$ , while the highest average thickness was measured in specimen #1, amounting to 148.57  $\mu\text{m}$ . The porosity rate in the coating was also determined, amounting to about 2%. TiC and TiB<sub>2</sub> particles were relatively large, while their volume fraction in the coating was 60 to 65%. They varied in size and were distributed throughout the coating as anticipated.

The region under the resulting coating is known as the laser melt zone (LMZ). Measurements of the thickness of the laser melt zone revealed that the thickness increased with greater energy input and higher overlapping rate. Due to heat transfer during the coating process and the melting of the substrate, the thickness also increased linearly through the cross-section in the direction of the coating application. The thickness of the laser melt zone, measured in the middle of the coated specimen, amounted from

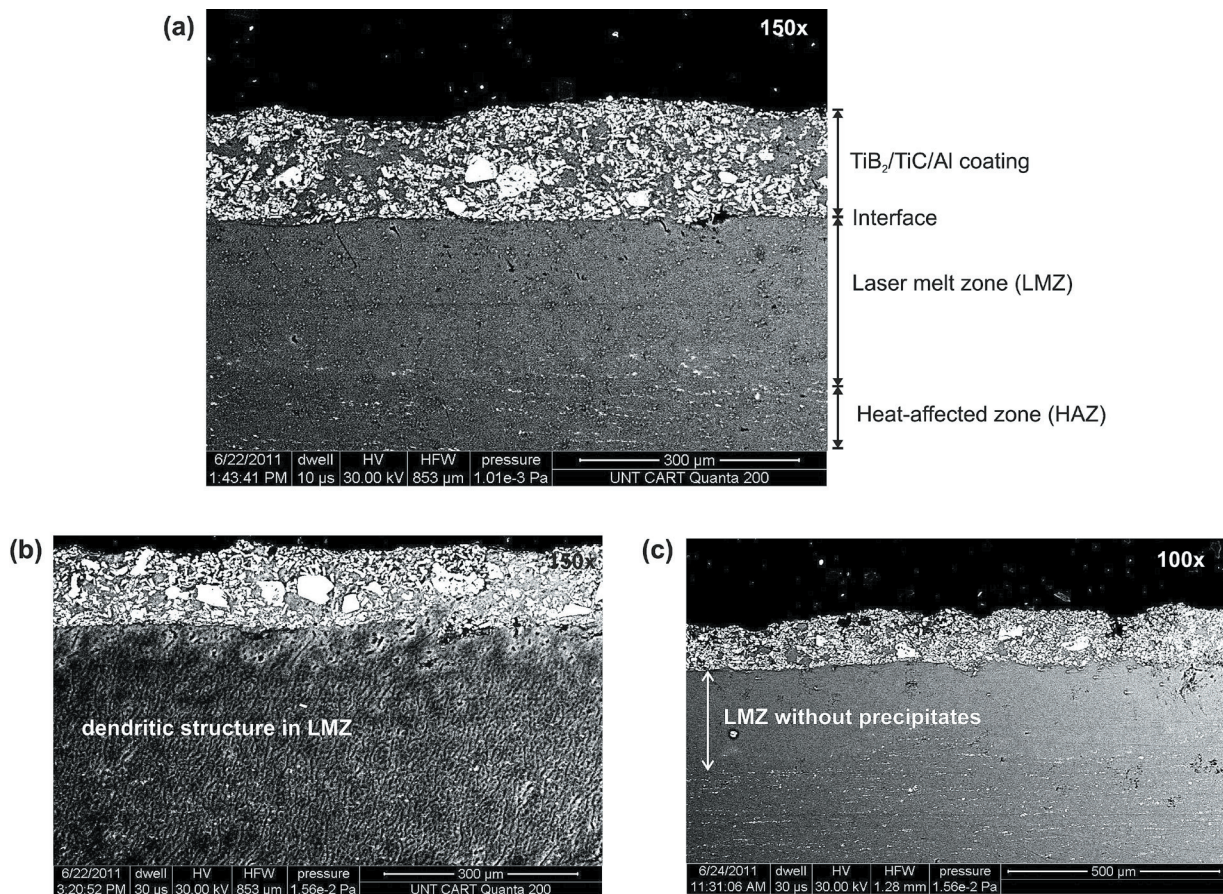


Fig. 1. a) SEM image of the laser-coated layer, b) dendritic microstructure in LMZ, c) reduced number of precipitates in LMZ

207.65 to 347.80  $\mu\text{m}$ , with regard to different coating conditions. The laser melt zone shown in Fig. 1b illustrates a cellular dendritic microstructure, typical of cast aluminium alloys. These findings indicate that during the coating process, a temperature high enough to cause complete melting of the substrate surface appeared under the coating. Due to rapid local solidification, the surface transformed into a dendritic structure [15]. The size of the resulting dendrites in the laser melt zone depended on the temperature of the melt during heating, and on the cooling rate. The cooling rates gradually decreased with the depth of the laser melt zone. Therefore, a fine dendritic microstructure emerged on the substrate surface, where the cooling rate was the highest, and was transformed into a coarse structure with greater LMZ depth [15]. Due to the overheating of the substrate during the coating process, no precipitates seemed to appear in the LMZ or their number significantly decreased, as shown in Fig. 1c. A lower number of precipitates of greater sizes was observed in the heat-affected zone (HAZ). In the region with a reduced number of precipitates, poorer mechanical properties may be anticipated.

Due to the large differences in the melting points of titanium carbide, titanium diboride and aluminium, the added aluminium powder and then also the aluminium alloy, i.e. the substrate, began melting as the laser beam acted on the coated surface. The thickness of the re-melted layer on the surface of the substrate just beneath the coating depended mainly on the laser coating conditions. Poor conductivity of the ceramic coating resulted in the major part of the laser beam energy being consumed for the heating of the coating, whereas only a small proportion of this energy was used for the melting of aluminium. Due to the capillary effect during the remelting process, the molten aluminium filled the pores between ceramic components. A sufficiently high energy density may cause the dissolution of  $\text{TiC}$  and  $\text{TiB}_2$  particles, and the occurrence of new phases. Upon the dissolution of  $\text{TiB}_2$ , a new phase  $\text{AlB}_2$  [16] may occur, whereas upon the dissolution of  $\text{TiC}$ , phase  $\text{Al}_4\text{C}_3$  [5] occurs. Since  $\text{TiB}_2$  has more free energy than  $\text{TiC}$ , it is more resistant at higher temperatures. Therefore, it is more likely that phase  $\text{Al}_4\text{C}_3$  will occur rather than phase  $\text{AlB}_2$ .

The Ti-B binary phase diagram is presented in Fig. 2. Two intermetallic compounds exist:  $\text{TiB}$  and  $\text{TiB}_2$ . According to the phase diagram, there is an additional intermetallic phase formed through peritectic reaction:  $\text{Ti}_3\text{B}_4$ . The phase  $\text{TiB}_2$  is a congruent melting phase, and is also thermodynamically stable in the aluminium

melt. Consequently, there are no reaction products present. The transfer of B and Ti into the aluminium melt normally goes through fluoride salts ( $\text{K}_2\text{TiF}_6$  and  $\text{KBF}_4$ ) [17]. With further cooling of such a melt, a relatively thermodynamically stable composite is normally expected. The transfer of B, Ti and C atoms can cause a local inhomogeneity or a super-saturation effect. This results in the formation of different precipitations after additional thermal treatment.

Fig. 3 shows the results of a microchemical surface analysis for C, Al, Ti and B for specimen #12. The specimen was coated with a 60 / 20 / 20 ratio of clad material, an overlapping rate of 30% and an energy density of 20  $\text{J}/\text{mm}^2$ . In Fig. 3, an interface between the substrate and the composite is visible.

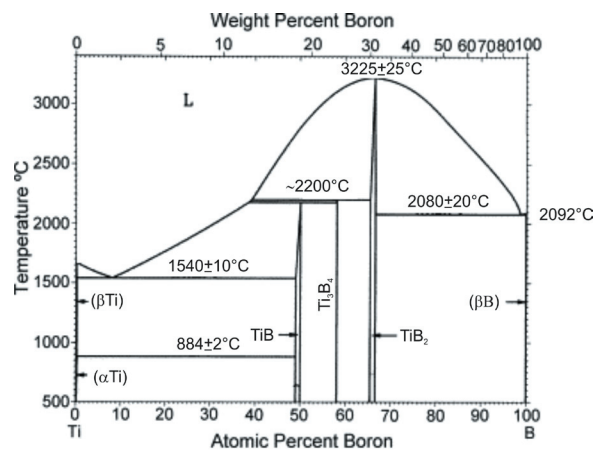


Fig. 2. Ti-B binary phase diagram [18]

As anticipated, aluminium was found as a part of the substrate as well as a part of the composite material around facets. Carbon was found to occupy spots alongside the aluminium. It is assumed that after the decomposition of  $\text{TiC}$ , carbon bonds with aluminium and forms aluminium carbide  $\text{Al}_4\text{C}_3$ . Elements Ti and B were found in the regions of facets, assumed to be a part of titanium diboride. It was not possible to define which of the facets are  $\text{TiC}$  and  $\text{TiB}_2$  in our study, as was the case in the study of Du [19]. The distribution of elements in that study reveals that the concentration of titanium is found in both the rectangular and spherical types of facets. The concentration of B and C was found in rectangular and spherical facets, respectively. These results give us an indication that the rectangular facets are related to the presence of  $\text{TiB}_2$  and the spherical ones with  $\text{TiC}$ .

Qualitative analysis was performed in designated measuring positions, illustrated in Figs. 4a and b. Because the specimen coating was electrically non-conductive, the surface of the coated specimens

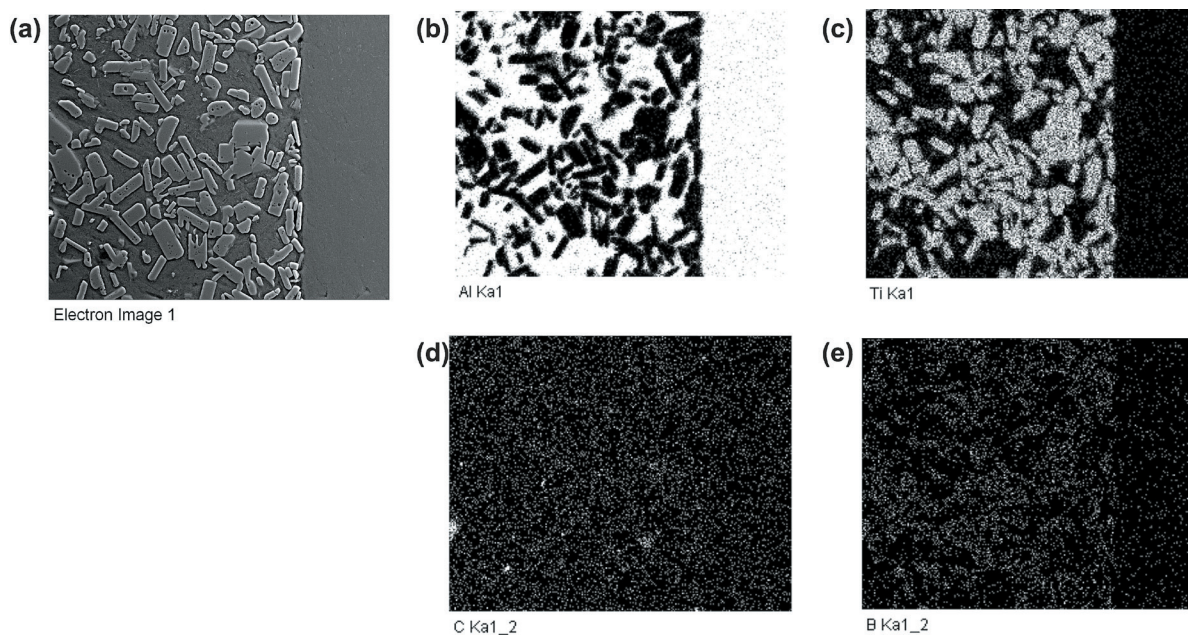


Fig. 3. a) SEM microphotographs and corresponding distribution of elements, b) aluminium, c) titanium, d) carbon and e) boron

was sprayed with a thin layer (7 nm) of carbon. Using EDS analysis, six elements were identified in the coating: Al, Ti, B, C, O and Si. Table 4 shows individual measuring positions in the coating with various elements, on the basis of which the presence of different phases may be inferred. Due to the prior deposition of carbon on the specimen surface, carbon wt.% values were not shown, since they would not represent the real results.

It was established on the basis of a preliminary analysis that measuring positions with no facets present, i.e. in spectra 6, 7 and 9, contained carbon and aluminium, as well as oxygen and small amounts of titanium and silicon. Since Al, O and C were in proximity to each other, this could affect the occurrence of aluminium oxycarbide. Titanium present in the aluminium substrate represented the basis for the occurrence of phase  $\text{Al}_3\text{Ti}$ , whereas the presence of boron could have resulted in the appearance of  $\text{TiB}$ ,  $\text{TiB}_2$  and / or  $\text{Ti}_3\text{B}_4$ . Silicon was a part of the chemical composition of the substrate and indicated that the coating was mixed with the substrate during the coating process; some amount of silicon was transferred into the coating. Other possible elements were all under the detection limit. Thus, no other reflections were noticed, and the presence of other complex intermetallic phases, especially magnesium and compound  $\text{Mg}_2\text{Si}$ , could be eliminated.

Qualitative analysis of smaller facets in spectra 2, 3, 4, 5, 10, 12 and 13 indicated a greater content of

titanium and boron, probably confirming the existence of  $\text{TiB}_2$ . The smaller part of aluminium is attributed to the background of the electron beam. It should be emphasized that titanium has a stronger signal compared to boron, because of a higher electron dissipation level ( $M_t = 204.38 \text{ g/mol}$ ).

Table 4. EDS results given in wt. %

Meas. position	B	Al	Ti	O	Si
Spec.1		2.91	74.16		
Spec.2	26.92	2.28	45.46		
Spec.3	26.41	2.11	43.83		
Spec.4	27.71	2.17	46.87		
Spec.5	30.42	2.86	43.12		
Spec.6		68.46	0.69	2.74	0.50
Spec.7		63.78	0.69	2.38	0.42
Spec.8		3.20	75.33		
Spec.9		82.90	1.13	2.17	0.44
Spec.10	24.73	1.91	43.15		
Spec.11		3.57	66.36		
Spec.12	25.85	2.40	43.21		
Spec.13	24.02	2.01	43.85		

The results of the analysis of a smaller facet in spectrum 11 were similar to results of the analysis of bigger facets in spectra 1 and 8, where there was a higher content of titanium. In the proximity of this phase, however, there were no reaction products, such as  $\text{Al}_3\text{Ti}$  or  $\text{Al}_4\text{C}_3$ . Thus, the smaller content of aluminium was considered to be a signal from the

aluminium matrix. The presence of carbon in facets 1, 8 and 11 indicated the existence of TiC.

In this regard, Liang et al. [20] report that the phase type may be determined on the basis of the facet shape. They agree with Du et al. [19], who claim that elongated or rectangular particles belong to  $TiB_2$ , whereas the spherical particles belong to TiC. In our case, this statement could be agreed upon, except in spectrum 11, where no boron was present. Therefore, it could not be claimed that the rectangular and elongated facet in spectrum 11 confirms the presence of  $TiB_2$ .

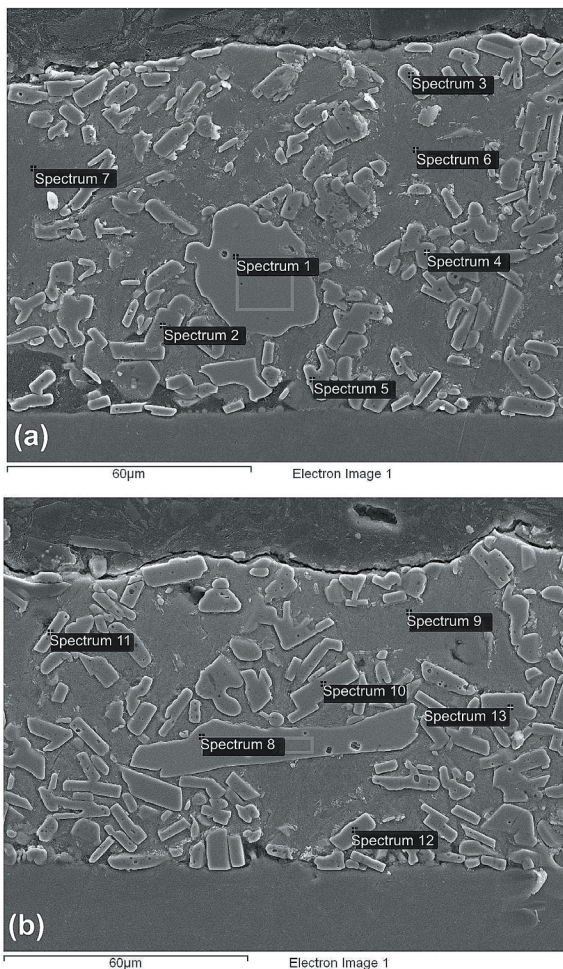


Fig. 4. Selected and measured regions using EDS analyses of: a) specimen #4, and b) specimen #10

## 2.2 Thermodynamic Analysis

If Ti is present in pure aluminium (or alloy) in a smaller excess, the occurrence of phase  $Al_3Ti$  is possible. The method in which the phase is formed

depends on the technology. The  $Al_3Ti$  phase is most commonly formed through the reaction between TiC and Al, where  $Al_4C_3$  is also possible. Normally, this latter carbide is formed by precipitation from the solid aluminium matrix. In the three component system T-C-Al (viewed from the aluminium rich-side perspective), the phase TiC decomposes to  $Al_3Ti$  and  $Al_4C_3$  at higher temperatures. By adding TiB and TiC to the aluminium alloy, phase equilibrium is possible as calculated in Fig. 5. The isopleth phase diagram Al-Mg is presented in Fig. 5. The equilibrium thermodynamic calculation was made for the system in which the aluminium alloy and the coating were in ratio EN AW-6082 : TiB = 4 : 1.

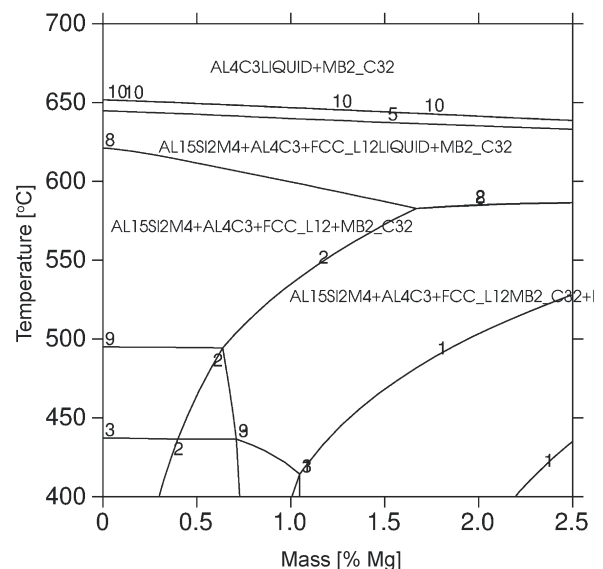


Fig. 5. Equilibrium isopleth phase diagram of Al-Mg for ratio ENAW 6082: TiB = 4 : 1

It can be inferred from the thermodynamic calculation that (together with the standard phases, which usually occur in alloy EN AW-6082) two new phases occurred as well:  $TiB$  ( $MB2\_C32\#1$ ) and  $Al_4C_3$  ( $AL4C3\#1$ ). In the final equilibrium state, all of the boron will react with the titanium, and all of the carbon with the aluminium.

Nevertheless, the  $Al_4C_3$  phase is difficult to detect on the surface of the coating, as concluded in the research of Dubourg et al. [5]. Although the melting point of TiC is higher than the evaporation temperature of aluminium, the dissolution of TiC is possible due to a higher absorption coefficient of TiC. That is why TiC can decompose; meanwhile, aluminium powder stays in its dissolved state and causes further formation of the  $Al_4C_3$  phase [5].

### 2.3 Thermal Analysis

In order to confirm the appearance of different phases with different ratios of ceramic components during the laser coating process, a thermal analysis was conducted. The measurement was performed under protective gas Ar with a purity degree of 5 and constant flow through the furnace. An empty corundum crucible was used as a reference. The maximum temperature reached was 550 °C using 10 K/min of heating/cooling rate. DSC (differential scanning calorimetry) was performed for two specimens with designations #3 and #9. Fig. 6 illustrates two DSC heating curves for both specimens. In both cases, two exothermic peaks were observed, which are typical for the precipitation of phases in solid state. The first thermal effect in both cases was detected at a temperature of about 215 °C, whereas the second thermal effect occurred at a slightly higher temperature, i.e. about 410 °C. The slope of the second thermal effect is much more distinctive for both samples and indicates that the process of the first thermal effect is less intensive. Because both peaks were found in a specific temperature interval, we can assume that the precipitation was gradual. Such peaks can be found in the case of precipitation of Mg<sub>2</sub>Si and Al<sub>6</sub>Mn for a particular aluminium alloy 6082. Such intense peaks can be found with relatively low concentrations of magnesium (under 0.8 wt.%).

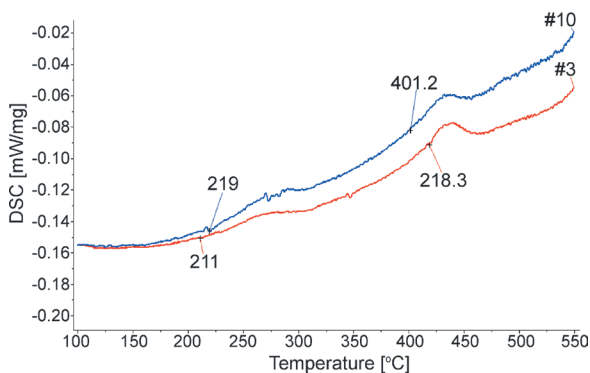


Fig. 6. DSC heating curves

### 2.3 Microhardness

The Vickers hardness tests were performed on a Leitz-Wetzlar tester to determine the microhardness value of the coating and in the depth under a load of 100 g and indentation time of 15 s. The measurement of the hardness of the coating was conducted at a half thickness of the coating. Sixteen iterations were performed horizontally in a randomly selected

position, at intervals of 500 μm. Microhardness values were also measured along the depth in increments of 50 μm to the depth of 900 μm. The greatest measuring depth was determined with regard to the depth of LMZ and HAZ. The HAZ was less prominent, since the specimen was heated at a temperature higher than precipitation only for a short period of time. The chosen method of microhardness measurement confirmed the differences in the microstructure of individual regions.

Fig. 7 illustrates the profile of microhardness along the depth of the coated specimens with the energy density of 13.3 J/mm<sup>2</sup> at different overlapping rates 30 and 50% and both ratios of clad material, and with pertaining standard deviation. Due to differences in the coating thickness, the coordinate origin of the depth is placed at the coating-substrate interface. The microhardness value of the aluminium alloy prior to the application of the coating was 96.6 HV<sub>0.1</sub>. Following the coating process, this value increased on average by 66% with regard to the selected powders and laser coating parameters. The value thus amounted to around 160 HV<sub>0.1</sub>. Due to different sizes of TiC and TiB<sub>2</sub> particles and their uneven distribution in the coating, there was a wide spread of microhardness results. Therefore, the results of measurements largely depended on the measuring position in the coating with regard to individual phase types. However, the microhardness values in the case of 30% overlapping are apparently higher than with 50% overlapping. Furthermore, the microhardness values in the case of 40 / 40 / 20 are slightly higher than 60 / 20 / 20. Measuring microhardness along the depth proved that higher heat input during the coating process results in lower microhardness values in the LMZ and HAZ. Thus, higher energy density and higher overlapping rate decreased the microhardness values in the LMZ and HAZ in the substrate under the coating surface. The average microhardness value in LMZ was 66.6 HV<sub>0.1</sub>, whereas this value amounted to 71.6 HV<sub>0.1</sub> in the HAZ. This was a significantly lower value than the microhardness value of the aluminium alloy, i.e. 96.6 HV<sub>0.1</sub>, prior to the coating process.

Lower microhardness values in the LMZ and in the HAZ may be attributed to changes in the substrate microstructure, resulting from thermal effects during the coating process and thus contributing to the process of homogenization and incomplete precipitation annealing in the LMZ and HAZ. Partial homogenization on the substrate surface could be attributed to the rapid coating process. Some of the Si underwent forced dissolution, while some of it remained in the form of Mg<sub>2</sub>Si precipitates

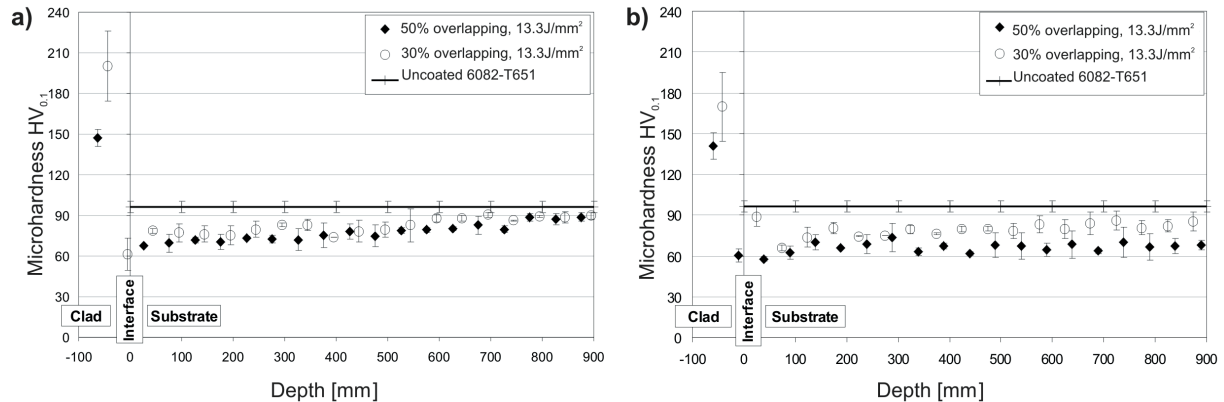


**Fig. 7.** Profile of microhardness along the depth, following the coating process with the energy density of  $13.3 \text{ J/mm}^2$  and two ratios of clad material; a) 40 / 40 / 20, and b) 60 / 20 / 20 at different overlapping rates 30 and 50%

in the laser melt zone. After a certain period of ageing, the oversaturated solid solution started to precipitate fine sub-microscopic particles in the form of intermetallic compounds, especially within the crystal grains, resulting in the formation of internal stress on a crystalline level, and preventing the grains from moving, thus causing higher hardness values. Therefore, subsequent heat treatment by means of solution annealing and artificial ageing in a furnace made it possible to improve the microstructure, microhardness and thus also the mechanical properties of the LMZ and HAZ. DSC heating curves also indicated the existence of precipitates in the substrate, resulting from subsequent heat treatment of the coated specimens. Thus, the microhardness values in the LMZ and HAZ were higher.

### 3 CONCLUSIONS

The research presents the laser coating of the 6082-T651 aluminium alloy with different contents of ceramic components ( $\text{TiB}_2$ -TiC) and the addition of aluminium (Al) in order to improve chemical bonding between the coating and the substrate at different overlapping rates and energy densities. Results and analyses conducted on different coatings applied to aluminium alloys corroborate the following conclusions:

- Results of microstructural analysis confirmed that a quality coating with good adhesion to the substrate was obtained in all cases. The average coating thickness was  $130 \mu\text{m}$  at an average porosity lower than 2%, corresponding to demanding applications. In all cases, good adhesion of the coating to the substrate was obtained.

- In both cases of ceramic components with the addition of Al, the average coating microhardness value obtained at different combinations of laser coating conditions was  $160 \text{ HV}_{0.1}$ , which represented a 66% higher microhardness value than that of the uncoated aluminium alloy. Measurements of microhardness of the substrate surface under the coating revealed that the heat during the remelting process affected the microstructural changes in the substrate and resulted in lower microhardness values. The average microhardness value in the LMZ was  $66.6 \text{ HV}_{0.1}$ , whereas in the HAZ, the value was  $71.6 \text{ HV}_{0.1}$ . The results show that at higher energy densities and higher overlapping rates, lower microhardness values were obtained in the LMZ and HAZ.
- Thermodynamic calculation shows that, in the final equilibrium state, all of the boron will react with the titanium, and the entire carbon with the aluminium. EDS analysis conducted in the coating revealed that a new phase, called oxycarbides, could form in the matrix.
- Thermal analysis, during which the coated specimens were heated to  $550 \text{ }^\circ\text{C}$ , confirmed the existence of two separate exothermic peaks at temperatures of  $215$  and  $410 \text{ }^\circ\text{C}$ . It can be inferred from the peaks in the heating curve that these two exothermic peaks were related to gradual precipitation. Since the EDS analysis did not reveal the presence of Mg and Mn in the coating, it was concluded that gradual precipitation occurred in the substrate, i.e. in the LMZ and HAZ.

## 4 ACKNOWLEDGMENTS

The authors gratefully acknowledge Prof. Narendra B. Dahotre and his research group from the Laboratory for Laser Materials Synthesis and Fabrication, Department of Materials Science and Engineering, University of North Texas, Denton, Texas, USA, for carrying out the laser coating.

## 5 REFERENCES

- [1] Žagar, S., Grum, J. (2011). Surface Integrity after mechanical hardening of various Aluminium alloys. *Strojniški vestnik – Journal of Mechanical Engineering*, vol. 57, no. 4, p. 334-344, DOI:10.5545/sv-jme.2010.092, DOI:10.5545/sv-jme.2010.092.
- [2] Trdan, U., Grum, J. (2012). Evaluation of corrosion resistance of AA6082-T651 aluminium alloy after laser shock peening by means of cyclic polarisation and EIS methods. *Corrosion Science*, vol. 59, p. 324-333, DOI:10.1016/j.corsci.2012.03.019.
- [3] Trdan, U., Porro, J.A., Oca-a, J.L., Grum, J. (2012). Laser shock peening without absorbent coating (LSPwC) effect on 3D surface topography and mechanical properties of 6082-T651 Al alloy. *Surface & Coatings Technology*, vol. 208, p. 109-116, DOI:10.1016/j.surfcoat.2012.08.048.
- [4] Sušnik, J., Šturm, R., Grum, J. (2012). Influence of laser surface remelting on Al-Si alloy properties. *Strojniški vestnik – Journal of Mechanical Engineering*, vol. 58, no. 10, p. 614-620, DOI:10.5545/sv-jme.2012.696.
- [5] Katipelli, L.R., Agarwal, A., Dahotre, N.B. (2000). Laser surface engineered TiC coating on 6061 Al alloy - microstructure and wear. *Applied Surface Science*, vol. 153, no. 2-3, p. 65-78, DOI:10.1016/S0169-4332(99)00368-2.
- [6] Chong, P.H., Man, H.C., Yue, T.M. (2002). Laser fabrication of Mo-TiC MMC on AA6061 aluminum alloy surface. *Surface and Coating Technology*, vol. 154, no. 2-3 p. 268-275, DOI:10.1016/S0257-8972(01)01719-4.
- [7] Anandkumar, R., Almeida, A., Colaco, R., Vilar, R., Ocelik, V., De Hosson, J. Th. M. (2007). Microstructure and wear studies of laser clad Al-Si/SiC(p) composite coatings. *Surface & Coatings Technology*, vol. 201, no. 24, p. 9497-9505, DOI:10.1016/j.surfcoat.2007.04.003.
- [8] Dubourg, L., Ursescu, D., Hlawka, F., Cornet, A. (2005). Laser cladding of MMC coatings on aluminium substrate: influence of composition and microstructure on mechanical properties. *Wear*, vol. 258, no. 11-12, p.1745-1754, DOI:10.1016/j.surfcoat.2007.04.003.
- [9] Čekada, M., Panjan, P. (2004). Laser methods for surface protection. *Vakuumist*, vol. 24, no. 4, p. 4-10. (In Slovene)
- [10] Anandkumar, R., Almeida, A., Vilar, R. (2011). Wear behavior of Al-12Si/TiB<sub>2</sub> coatings produced by laser cladding. *Surface and Coatings Technology*, vol. 205, no. 13-14, p. 3824-3832, DOI:10.1016/j.surfcoat.2011.01.048.
- [11] Uenishi, K., Kobayashi, K.F. (1999). Formation of surface layer based on Al<sub>3</sub>Ti on aluminum by laser cladding and its compatibility with ceramics. *Intermetallics*, vol. 7, no.5, p. 553-559, DOI:10.1016/S0966-9795(98)00071-5.
- [12] Brandes, E.A., Brook, G.B. (1998). *Smithells Light Metals Handbook*. Butterworth-Heinemann, Oxford.
- [13] European Aluminum Association and the Matter Project, from <http://aluminum.matter.org.uk/aluselect/>, accessed on 2012-04-16.
- [14] BS EN 485-2:2004. (2004). *Aluminium and aluminium alloys - Sheet, strip and plate - Part 2: Mechanical properties*. British standard Institution, London.
- [15] Kadolkar, P., Dahotre, N.B. (2002). Variation of structure with input energy during laser surface engineering of ceramic coatings on aluminium alloys. *Applied Surface Science*, vol. 199, no. 1-4, p. 222-233, DOI:10.1016/S0169-4332(02)00799-7.
- [16] Xu, J., Li, Z., Zhu, W., Liu, Z., Liu, W. (2007). Investigation on microstructural characterization of in situ TiB/Al metal matrix composite by laser cladding. *Materials Science and Engineering A*, vol. 477, no. 1-2, p. 307-313, DOI:10.1016/j.msea.2006.10.057.
- [17] Lakshmi, S., Lu, L., Gupta, M. (1998). In situ preparation of TiB<sub>2</sub> reinforced Al based composites. *Journal of Materials Processing Technology*, vol. 73, no. 1-3, p. 160-166, DOI:10.1016/S0924-0136(97)00225-2.
- [18] Murray, J.L., Liao, P.K., Spear, K.E. (1987). The Ti-B (titanium-boron) system. Murray, J.L. (ed.), *Phase Diagrams of Binary Titanium Alloys*. ASM International, Metals Park, p. 33-38.
- [19] Du, B., Zou, Z., Wang, X., Li, Q. (2007). In situ synthesis of TiC-TiB<sub>2</sub> reinforced FeCrSiB composite coating by laser cladding. *Surface Review and Letters*, vol. 14, p. 315-319, DOI:10.1142/S0218625X07009414.
- [20] Liang, Y., Han, Z., Zhang, Z., Li, X., Ren, L. (2012). Effect of Cu content in Cu-Ti-B<sub>4</sub>C system on fabricating TiC/TiB<sub>2</sub> particulates locally reinforced steel matrix composites. *Materials and Design*, vol. 40, p. 64-69, DOI:10.1016/j.matdes.2012.03.023.